Mismatched Wavelets: Information Hiding and Edge Detection

Christopher B. Smith and Sos S. Agaian

***Abstract*— Wavelets and other tight frames have been used for numerous signal and image processing applications. These transforms consist of two or more filters that are applied in "analysis" and "synthesis" operators. In general, these operators are designed such that perfect reconstruction is preserved.**

This paper introduces mismatched wavelets, in which analysis and synthesis operators do not form a perfect reconstruction system. Rather than minimize the errors introduced by such a system, we study and exploit these errors. These structured errors are far from random, preserving much of the informational structure of the image. Two applications, data hiding and edge detection, are shown that can effectively exploit these errors. Computer simulations show promise compared to several common techniques. These errors can also be used in a variety of applications, including copyright protection for digital media, content authentication, media forensics, data binding covert communications, and other image processing fields.

***Index Terms*—Wavelets, mismatched wavelets, visual similarity, edge detection, information hiding**

I. Introduction

Wavelets and, more recently tight frames, have become powerful tools for the advancement of many areas in signal and image processing. The multiresolution structure of the discrete wavelet transform (DWT) coupled with the existence of fast implementations make the DWT an excellent tool for many tasks. [1]-[3] In general a wavelet or framelet based signal or image processing system consists of 3 stages, 1) the forward transform, 2) some processing on the coefficients, and 3) the inverse transform; along with ancillary pre- and post-processing stages. For example, a wavelet based edge detection algorithm can be created by (1) Perform full forward transform, (2) Delete lowpass wavelet coefficients, (3) Perform inverse transform, and (4) Use thresholding to remove remaining highpass noise.

A simple technical description of a wavelet can be found in the two channel filterbank representation. In this form, the wavelet transform is performed by two orthogonal filters applied in a cascade of decimation and filter stages. By tradition these have been called the "scaling" and "wavelet" filters, or "father" and "mother" wavelets. These filters are used in both the forward and inverse wavelet transforms, known as "analysis" and "synthesis" operators. For a perfect reconstruction system, the analysis and synthesis operators use the same set of filters.

In the biorthogonal wavelet transform, non-orthogonal wavelet filters are used for highpass and lowpass components. To preserve perfect reconstruction, the analysis and synthesis operators are changed, but still related to one [1] A tight frame based system is again similar, but not restricted to two channels. These are again applied using analysis and synthesis operators that preserve perfect reconstruction. For an overview of these applications see [4]-[7].

Over the years several techniques have been developed for the design of near-perfect reconstruction filter banks [8]. In the mid-1990s Nguyen proposed the near-perfect reconstruction filterbank[9]. The goal of this research was to construct a pseudo-quadrature mirror filterbank that trades perfect reconstruction (PR) for better stop band attenuation, improving filter quality while minimizing errors introduced. [8]-[13]. By relaxing the PR requirements, nearly perfect reconstruction filter banks can be designed with less complexity and more selectivity [13] as well as for performance in specialized applications [14].

In this paper we present a variation on the wavelet transform called mismatched wavelets. We partner analysis and synthesis steps into a non-perfect reconstruction (NPR) system and rather than minimize the errors, we study and exploit the errors introduced. Far from being random, these errors have properties that are useful in two major applications, information hiding and edge detection. The first application is data hiding in digital images. In data hiding applications there are two primary practical considerations: security and embedding efficiency. To address these two issues, this approach uses the errors introduced by mismatched wavelets to locate areas of an image in which embedding information will preserve the visual and statistical properties of the image. This approach is novel and shows potential for high data rate,

Manuscript received March 2011. This work was supported in part by Presidential Discretionary funding from Southwest Research Institute and the Center for Infrastructure Assurance and Security at University of Texas San Antonio.

C. B. Smith is with Southwest Research Institute, 6220 Culebra Road, San Antonio, TX 78238, and the Department of Electrical and Computer Engineering, University of Texas San Antonio, 6900 North Loop 1604 West, San Antonio, TX 78249 USA (phone: 210-522-5981; fax: 210-522-2719; e-mail: cbsmith@ieee.org).

S. Agaian, is with the Department of Electrical and Computer Engineering, University of Texas San Antonio, 6900 North Loop 1604 West, San Antonio, TX 78249 USA and Tufts University, Medford, Massachusetts, USA (phone: 210-458-5939 Fax: 210-458-5947 e-mail: sagaian@utsa.edu).

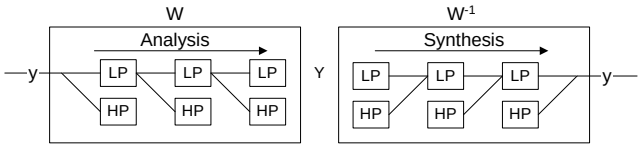

Figure 1, Wavelet transform, analysis and synthesis stages

secure embedding. Several examples are shown including comparative results.

The second application is a fundamental problem in image processing, the detection of edges. Edges are discontinuities in intensity due to changes in image information. One of the major goals of edge detection is to capture the information in the image in as compact a form as possible. This is typically done using an estimate of a gradient followed by a thresholding operation to isolate the edges of an image. This paper introduces a novel edge detector based on the information-preserving errors introduced by mismatched wavelets. This approach is different from typical wavelet-based edge detectors and can outperform these and other methods. Several comparative examples are shown in both qualitative and quantitative experiments. The authors believe that non-perfect reconstruction errors can further be used in a variety of applications, including copyright protection for digital media, content authentication, media forensics, covert communications, and other image processing fields.

In the Section II, we formally treat wavelets and the description of the mismatched wavelets, including the definition of distance between two wavelet filters and definition of the subclass of visually-similar mismatched wavelets. The following sections, III and IV, will demonstrate the use of mismatched wavelets for two applications, data hiding and edge detection, including comparative simulations. Finally, we close with some general conclusions and remarks.

II. Mismatched Wavelets

In this section mismatched wavelets are introduced. We begin by reviewing the basics of orthogonal, biorthogonal, and frame based wavelets. Based on this reference a measure is defined to quantify the distance between two wavelets. Mismatched wavelets are then introduced with a number of examples. We observe when filter pairs are "close" to one another, the changes made by this NPR system maintain the structure of the image. For smaller and smaller "distances", i.e. as the filters approach PR, the changes approach negligible levels. Using this property, we define visually similar mismatched wavelets.

A. Orthogonal, Biorthogonal, and Tight Frames

As discussed by Mallat and others, frame theory is the theory that analyzes discrete signal representations. A frame is a family of vectors, $\{\phi_n\}_{n\in\Gamma}$ on a possibly infinite index set Γ, that characterizes any signal f using its inner products $\{\langle f,\phi_n\rangle\}_{n\in\Gamma}$.

All wavelets including orthogonal and biorthogonal wavelets are tight frames, but not all tight frames are orthonormal wavelets. Of orthogonal, biorthogonal, and tight wavelet frames, the orthogonal wavelet is the most restrictive condition, enforcing a number of properties that are typically undesirable for applications, including non-symmetry or phase non-linearity.

A matrix form of the wavelet transform is often used as a notational convenience. In a matrix notation, let the analysis and synthesis operators as shown in Figure 1 be represented by W and W^{-1}. The forward wavelet transform or analysis operator based on ϕ_n be represented by W_{ϕ_n} for an orthogonal ϕ_n. Then we have $W_{\phi_n}W_{\phi_n}^T = I$ where explicitly, $W_{\phi_n}^{-1} = W_{\phi_n}^T$.

Biorthogonal wavelets also maintain perfect reconstruction, but approach phase linearity, using dual Riez bases to maintain perfect reconstruction. The analysis operator uses a scaling function, $\{\langle f,\phi_n\rangle\}_{n\in\Gamma}$, while the synthesis operator uses a different function $\{\langle f,\tilde{\phi}_n\rangle\}_{n\in\Gamma}$, with the restriction that $\langle\phi(t),\tilde{\phi}(t-n)\rangle = \delta[n]$ to maintain biorthogonality and perfect reconstruction. To formulate this in a matrix notation, $W_{\phi_n}W_{\tilde{\phi}_n}^T = I$, where explicitly, $W_{\phi_n}^{-1} = W_{\tilde{\phi}_n}^T$.

Tight frame wavelets, or framelets as termed by Daubechies, use a single function ϕ_n with multiple mother wavelets ψ_n to create a perfect reconstruction system. In a matrix form, $W_{\phi_n}W_{\phi_n}^{-1} = I$. Where $W_{\phi_n}^{-1} \neq W_{\phi_n}^T$.

This paper introduces a system which uses bases ϕ_n, and $\tilde{\phi}_n$ which do not preserve perfect reconstruction, i.e., $W_{\phi_n}W_{\tilde{\phi}_n}^{-1} \neq I$. Instead, we study the errors introduced when the bases used in analysis and synthesis are not matched. We use orthogonal wavelets as the basis to develop non-perfect reconstruction analysis tools. We base our work on orthogonal wavelets due to the ease of understanding and the wide availability of fast implementations. The same ideas can be applied using biorthogonal or tight frame approaches.

B. Wavelet Distance

For a formal definition of a mismatched wavelet, the concept of wavelet distance is needed. To define a distance, two different approaches are possible. First, a metric can be defined in terms of the results of the operators, i.e. the quality of the resulting image, and second, a metric can be defined based on the wavelet filters themselves.

1) Image Structural Similarity Measure

In the first case, we start with the results of the wavelet transform, defining the original image as i, the NPR transform results in,

$$W_{\phi_n} i W_{\tilde{\phi}_n}^{-1} = \hat{i}\,. \tag{2.1}$$

For the one-dimensional case or in the two-dimensional case,

$$\left(W_{\tilde{\phi}_n}^{-1}\left(W_{\phi_n} i W_{\tilde{\phi}_n}^{-1}\right)W_{\phi_n}\right) = \hat{i} \tag{2.2}$$

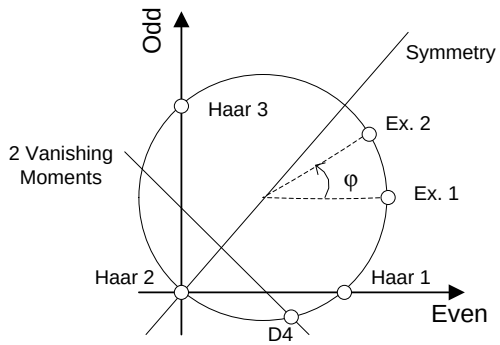

Figure 2, Odd and Even Wavelet space, demonstrates how Ex. 1 and Ex. 2 are a distance of $\varphi(\cdot)$ from one another

or for notational convenience $W_{\phi_n \phi_n'}(i) = \hat{i}$, which is a linear operator.

The ability to quantify the similarity or difference of i and $\hat{i}$ has been a topic of much research in the field of computer vision. As has been shown by Bovik, Simoncelli and a wide range of computer vision researchers [15]-[20], the measurement of image similarity is not a trivial problem. Common techniques of using the mean squared error (MSE) or peak signal to noise ratio (PSNR) have been shown to be poor methods of judging image quality. We define a measure of distance between two images, $M(i,\hat{i})$, such that visually similar images follow,

$$M(i,\hat{i}) < \varepsilon . \tag{2.3}$$

In [18][19], an image similarity measure is introduced that uses wavelet-like multiresolution analysis to decorrelate the image and capture image structure. Using the wavelet to capture the structural information of the image, the amount of information change is measured between two images using the structural similarity measure, SSIM, of the wavelet representation of an image.

$$SSIM(x,y) = \frac{\left(2\mu_x\mu_y + C_x\right)\left(2\sigma_{xy} + C_y\right)}{\left(\mu_x^2 + \mu_y^2 + C_x\right)\left(\mu_x^2 + \mu_y^2 + C_y\right)} \tag{2.4}$$

Though imperfect, this metric was shown to be among the state of the art in full reference image quality metrics [20], although the inclusion of higher-order statistics has been shown to be useful in steganography [25].

2) Analysis and Synthesis Operator Distance

It is desirable to define a metric between the analysis and synthesis operators themselves, ϕ_n and ϕ_n', i.e., $d(\phi_n, \phi_n')$. Using orthogonal wavelets as a baseline, we define this distance using parametric wavelets, i.e. a function that can generate wavelets. Pollen introduced a parameterization of orthogonal wavelets in [23]. For the four coefficient wavelet, his solution has the following form, where the parameter φ is used to generate new wavelets.

$$\begin{bmatrix} c_0 \\ c_1 \\ c_2 \\ c_3 \end{bmatrix} = \begin{bmatrix} \frac{1+\cos(\varphi)-\sin(\varphi)}{2} \\ \frac{1+\cos(\varphi)+\sin(\varphi)}{2} \\ \frac{1-\cos(\varphi)+\sin(\varphi)}{2} \\ \frac{1-\cos(\varphi)-\sin(\varphi)}{2} \end{bmatrix}, \tag{2.5}$$

To widen this definition to encompass additional tight frames as well as orthogonal wavelets, a different parameterization, introduced by Smith and Agaian [18], can be used,

$$\begin{bmatrix} c_0 \\ c_1 \\ c_2 \\ c_3 \end{bmatrix} = \begin{bmatrix} \frac{1 \pm \sqrt{1-4\varphi^2+4\varphi}}{2} \\ -\varphi+1 \\ \frac{1 \mp \sqrt{1-4\varphi^2+4\varphi}}{2} \\ \varphi \end{bmatrix}. \tag{2.6}$$

For simplicity, our discussion will continue with the Pollen parameterization.

To develop an understanding of this parameterization and how it can be applied as a distance measure, it is useful to explore Sweldens' space of odd and even coefficients of 4-coefficient filters shown in Figure 2. Sweldens [22], Heil, and others [24], divided the 4-coefficients c_k into two groups, "odd" and "even" coefficients. This leaves us with two degrees of freedom. We can choose them to be the first coefficient, termed "even" and the last one termed "odd". We then have:

$$c_0 = even, c_1 = 1-odd, c_2 = 1-even, c_3 = odd . \tag{2.7}$$

With the orthogonality constraint,

$$even \cdot (1-even) + odd \cdot (1-odd) = 0 , \tag{2.8}$$

this results in a circle in the space of even and odd, on which all orthogonal wavelets appear on a circle. The constraints of symmetry and maximal vanishing moments have a linear representation in this space.

Pollen's parameterization can be represented by an even periodic sampling of this circle of orthogonal wavelets. The parameter φ becomes an angular measure of distance between any two wavelets, as shown in Figure 2. That is the distance between any two scaling functions ϕ_n and ϕ_n' can be represented by,

$$d_P(\phi_n, \phi_n') = \left|\varphi(\phi_n) - \varphi(\phi_n')\right|, \tag{2.9}$$

where $\varphi(\cdot)$ is the parameter resulting in the basis, "$\cdot$".

C. Mismatched Wavelet Definition

To define mismatched wavelets, we start with the idea of *losing* perfect reconstruction, or

$$W_{\phi_n} W_{\phi_n'}^{-1} \neq I . \tag{2.10}$$

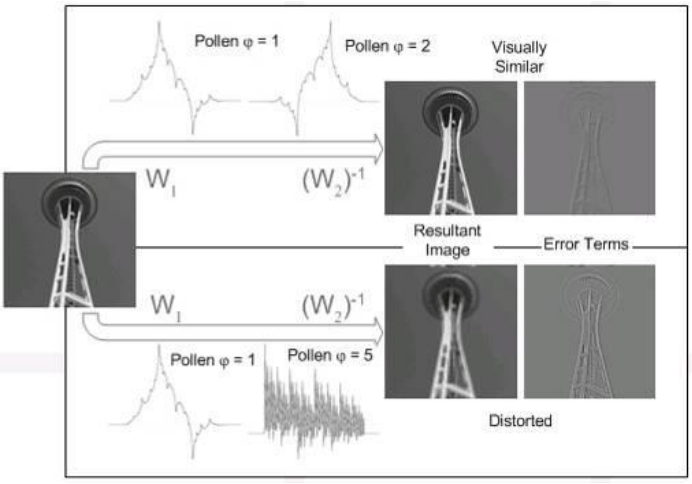

Figure 3, Mismatched wavelets and the error they introduce, include two forms, top the visually similar class of mismatched wavelets, and bottom the distortion inducing class of visually similar wavelets.

To maintain some reasonable behavior of the system we must choose ϕ_n and $\tilde{\phi}_n$, such that $W_{\phi_n} W_{\tilde{\phi}_n}^{-1} \approx I$. To do this in a systematic way, we use a distance measure $\rho = d_{\cdot}(\phi_n, \tilde{\phi}_n)$ between wavelet filters. Then it is desirable that,

$$\lim_{\rho \to 0} \left\langle \phi(t), \tilde{\phi}(t-n) \right\rangle = \delta[n]. \tag{2.11}$$

Using Pollen's parameterization distance, ρ becomes an angular measure of distance between any two wavelets, as discussed in Section II.B, i.e.,

$$\rho = d_P(\phi_n, \tilde{\phi}_n) \tag{2.12}$$

Definition: A system of operators is termed a *mismatched wavelet* system when the analysis and synthesis operators are (scaling functions) ϕ_n and $\tilde{\phi}_n$, alone form a complete multiresolution analysis, but together do not preserve perfect reconstruction; the errors of which can be exploited as a useful quantity.

Thus rather than a system of 3 stages, 1) the forward DWT, 2) some processing on the coefficients, and 3) the inverse transform; this new method is now a system of two stages, 1) forward DWT using ϕ_n, and 2) inverse DWT using $\tilde{\phi}_n$.

Mismatched wavelets can be generated using the Pollen parameterization. With this distance measure mismatched wavelets can be separated into those that result in visually similar errors and those which do not. We briefly introduced this idea in [18], but now present the full theory here.

D. Examples

Two example mismatched wavelets are shown in Figure 3. The visually similar case uses wavelets that are near mirror images of one another, (symmetry is not a requirement of the visually similar mismatched wavelet, but does provide a convenient example). For cases shown, the errors introduced by NPR retain much of the structure of the image, while the reconstructed image is perceptually identical to the original. In the distorted image shown, the errors again retain much of the image information, but in this case the reconstructed image is distorted. Examples from a number of other images can be found at the end of this paper.

E. Visual Similarity

To define a useful subclass of the mismatched wavelet, consider the case where the analysis and synthesis filters approach PR. In this case, the reconstructed image will be perceptually identical to the original. By using wavelets that are close to one another, we ensure the results will be similar to the original.

Definition: A system of analysis and synthesis operators is termed a *visually similar mismatched wavelet*, or *visually similar wavelet*, when the mismatched wavelet results in an image which is visually similar to the original.

Theorem: Corruptions due to mismatched wavelet filters result in small changes if the distance between analysis and synthesis operators is small.

The proof of which is trivial, if the distance $\rho = d_{\cdot}(\phi_n, \tilde{\phi}_n)$ between the wavelets is small,

$$\lim_{\rho \to 0} \left\langle \phi(t), \tilde{\phi}(t-n) \right\rangle = \delta[n] \tag{2.13}$$

implies $\lim_{\rho \to 0} W_{\phi_n} W_{\tilde{\phi}_n}^{-1} = I$, (2.14)

then $\lim_{\rho \to 0} W_{\tilde{\phi}_n \phi_n}(i) = i$, (2.15)

so given $\rho \approx 0$, $M(i, W_{\tilde{\phi}_n \phi_n}(i)) \approx 0$. (2.16)

This theorem can be extended informally to show visually similarity, using the SSIM defined in [19] applied in the wavelet domain,

$$SSIM(x,y) = \frac{\left(2\mu_x\mu_y + C_x\right)\left(2\sigma_{xy} + C_y\right)}{\left(\mu_x^2 + \mu_y^2 + C_x\right)\left(\mu_x^2 + \mu_y^2 + C_y\right)} \tag{2.17}$$

since, $E(\mathbf{vM}) = \mu_{\mathbf{v}} |\mathbf{M}|$, and

$$E\left(W_{\tilde{\phi}_n}^{-1} W_{\phi_n} i W_{\phi_n}^{-1} W_{\tilde{\phi}_n}\right) = \left|W_{\phi_n}^{-1} W_{\tilde{\phi}_n}\right| \mu_i \left|W_{\tilde{\phi}_n}^{-1} W_{\phi_n}\right| = \mu_i D_{\phi_n \tilde{\phi}_n},$$

Assigning,

$$\mathrm{var}\left(W_{\tilde{\phi}_n}^{-1} W_{\phi_n} i W_{\phi_n}^{-1} W_{\tilde{\phi}_n}\right) = E\left(\left(W_{\tilde{\phi}_n}^{-1} W_{\phi_n} i W_{\phi_n}^{-1} W_{\tilde{\phi}_n}\right)^2\right) + \left(\mu D_{\phi_n \tilde{\phi}_n}\right)^2 = \Sigma$$

Then,

$$SSIM(W_{\phi_n \tilde{\phi}_n}(i), W_{\phi_n \phi_n}(i)) = \frac{\left(2\mu_x D_{\phi_n \tilde{\phi}_n} \mu_y + C_x D_{\phi_n \tilde{\phi}_n}\right)\left(2\Sigma_{i W_{\phi_n} W_{\tilde{\phi}_n}^{-1}} + C_y\right)}{\left(\mu_x^2 D_{\phi_n \tilde{\phi}_n}{}^2 + \mu_y^2 + C_x D_{\phi_n \tilde{\phi}_n}\right)\left(\mu_x^2 D_{\phi_n \tilde{\phi}_n}{}^2 + \mu_y^2 + C_y D_{\phi_n \tilde{\phi}_n}\right)}$$

since, $W_{\tilde{\phi}_n}^{-1} W_{\phi_n} \approx I$, $D_{\phi_n \tilde{\phi}_n} \to 1$. As long as Σ is small, the errors introduced become visually undetectable.

In practice, the Pollen based distance less than one, i.e., $d_P(\phi_n, \tilde{\phi}_n) < 1$, has proven sufficient to maintain visual similarity. Figure 4 thru Figure 6 show the results applying a mismatched wavelet of distance, 0.01, 0.1, 0.5, and 1. Notice the differences in the images are not humanly discernable, while the first order statistics are virtually identical.

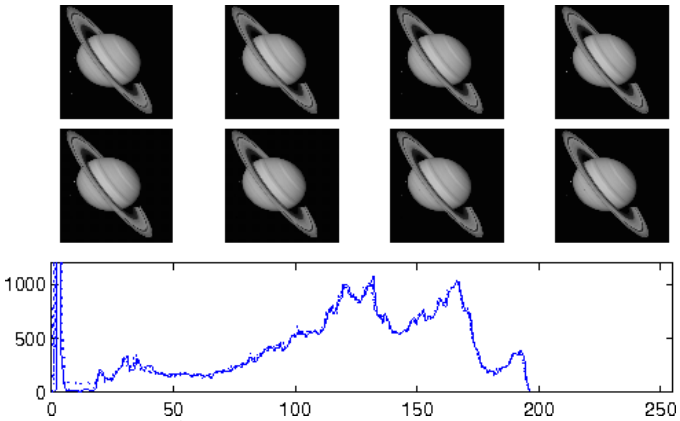

Figure 4, Results of generating visually similar images using a mismatched wavelet. From left to right distances of 0.01 0.1 0.5 1 are used. Bottom shows the histogram of each image, solid line is the original, dotted the visually similar version. The distortion induced by the mismatched wavelet does not visually distort the first order statistics.

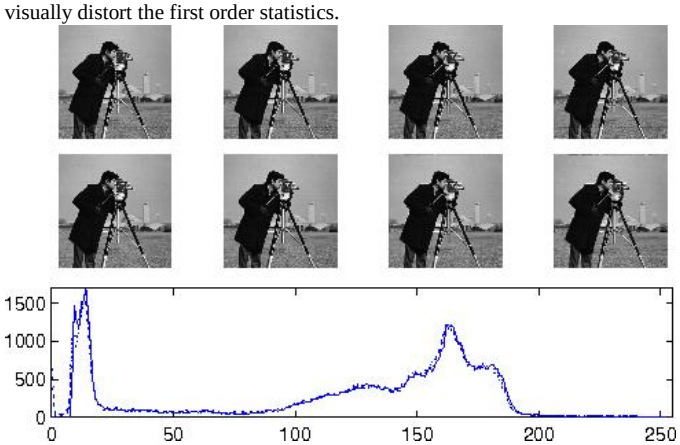

Figure 5, Results of generating visually similar images using a mismatched wavelet. From left to right distances of 0.01 0.1 0.5 1 are used. Bottom shows the histogram of each image, solid line is the original, dotted the visually similar version. The distortion induced by the mismatched wavelet does not visually distort the first order statistics.

F. Relationship to NPR QMF Banks, Multiwavelets, and Wavelet Packets

There are several topics in the literature that bear a cursory resemblance to the mismatchced wavelet. Just as the QMF bank is a generalization of the wavelet, so the pseudo-QMF, or NPR filterbank, is a generalization of the
mismatched wavelet. The goal of the NPR QMF research has been to trade PR for better stop band attenuation, improving filter quality while minimizing errors [8]-[13]. In this paper rather than minimize the errors, we study and exploit such. Multiwavelets and wavelet packets also bear some conceptual similarity to mismatched wavelets, though this similarity is superficial. Multiwavelets are a construction which results in multiple wavelet transforms being performed in an efficient parallel structure. Wavelet packets use different filters at each wavelet level, possibly decomposing high pass as well as low pass components. Both use filters in analysis and synthesis operators such that perfect reconstruction is preserved. The ideas presented here could benefit from extensions using either multiwavelets or wavelet packets but are independent in their own right.

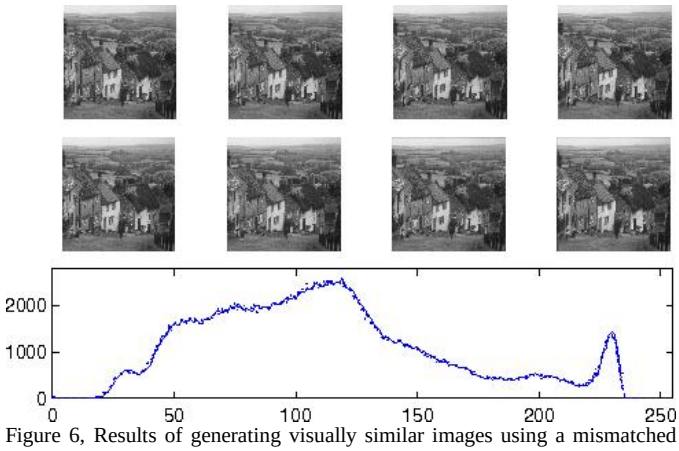

Figure 6, Results of generating visually similar images using a mismatched wavelet. From left to right distances of 0.01 0.1 0.5 1 are used. Bottom shows the histogram of each image, solid line is the original, dotted the visually similar version. The distortion induced by the mismatched wavelet does not visually distort the first order statistics.

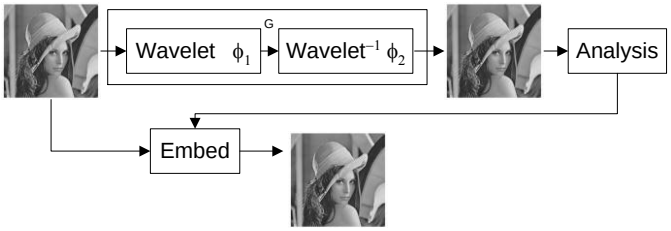

Figure 7, Mismatched wavelet based embedding, the distortion operator G is formed by using a mismatched pair of analysis and synthesis operators. Data is then embedded based on an analysis of the distorted image.

III. Information Hiding

In this section we introduce the idea of using mismatched wavelets to introduce distortions to an image while maintaining visually significant properties of the image. We further show how this can be applied to information hiding, with some comparative results.

A. Data Hiding

The problem in information hiding is how to modify a given image by embedding information, without making detectable changes to the image. A common example would be modifying the LSB of the image. In information hiding, such as steganography or watermarking, such simple techniques have been shown to be readily detectable [26]. In addition to simple techniques such as LSB modification, transform domain techniques are also prominent. Modifications in the transform domain introduce less perceptually obvious distortion than spatial techniques, but are also detectable [27]-[29]. The field of information hiding is a developing science; here we take a fundamentally different approach.

Instead of making a modification to the image, we generate an image that is visually and statistically similar to the original, then use the new image as a bound on how the original image can be modified. Such a process is shown in Figure 7. From Section II, we know the mismatched wavelet distortion channel will result in an image similar to the original. An embedding method is proposed based on an analysis of the image generated by mismatched wavelets. Since any bits modified by the mismatched wavelet are not visibly

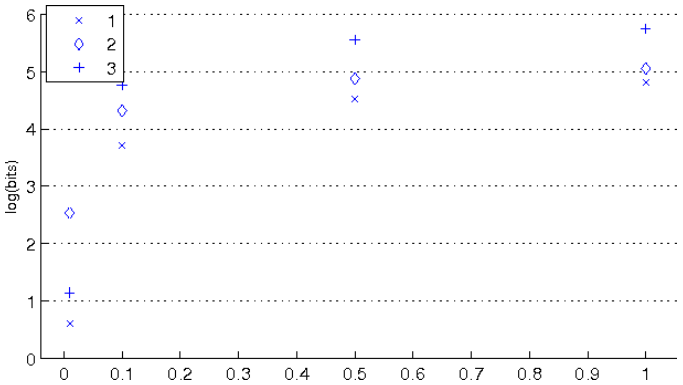

Figure 8: Bits made available by in the image generated by the mismatched wavelet, 1=Saturn, 2=Cameraman 3= Goldhill, on a log scale plotted against wavelet distance. All images are 512x512, distances used correspond to Figure 4-Figure 6. For the same images JSteg can only embed 1024 – 4096 bits.

significant, these bits can be replaced using any method desired. This transform-domain technique determines where to embed bits in the spatial domain. A brief exploration of other data hiding variations can be found in [18].

B. *Generating Similar Images*

To formulate the problem of generating similar images, we start with a natural image, *C*. To embed additional information into the image it must be passed through a distorting channel, G. The goal of information hiding is to construct that channel G such that the distortions applied to C are not detectable, i.e. the statistics of the distorted image are not different from typical image statistics.

Given a distortion model from [30],

$$D = GC + V, \tag{3.1}$$

the goal is to minimize the noise component introduced and derive a channel G such that G is close to identity. Using a channel composed of two mismatched wavelets eliminates the noise component, V, since there are no stochastic processes in such a system. The resulting channel

$$G = W_1 W_2^T, \tag{3.2}$$

in terms of wavelet matrices W_1, W_2. As discussed in Section II, the amount of distortion is now directly related to the distance between two wavelets, ρ. For example, this distance can be defined as the corresponding angle in the parametric wavelet. Given a distance ρ,

$$\lim_{\rho \to 0} W_1 W_2^{-1} = I \tag{3.3}$$

such that smaller distances introduce a less distorting channel. By choosing appropriate wavelets ϕ_n and $\hat{\phi}_n$, we can guarantee the distorting channel G produces minimal changes.

C. *Examples*

Numerous methods exist for embedding information into images, be it for watermarking or steganography. Here we present a method to determine "safe" locations and size of data to embed. Our goal is to demonstrate the viability of a new approach rather than create a cutting edged embedding algorithm. We compare the number and amount of data to the classic JSteg algorithm. Many newer approaches exist, but

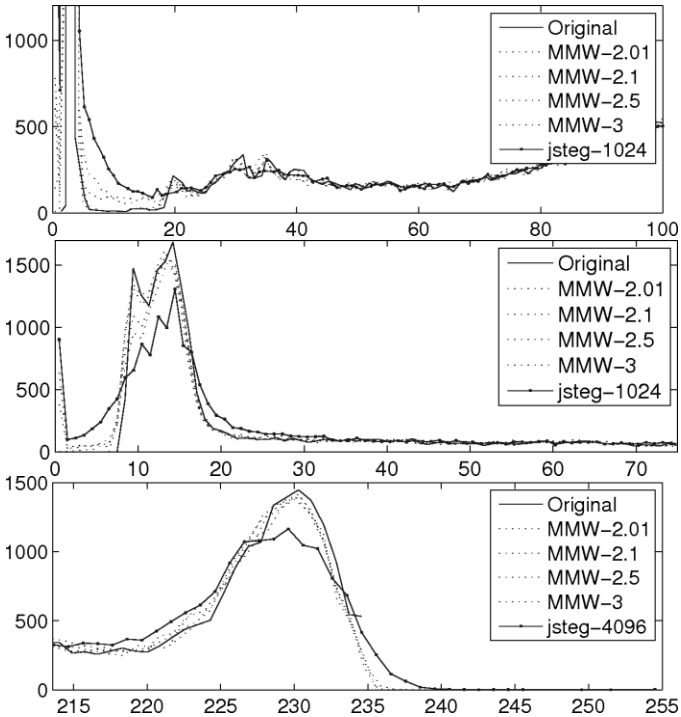

Figure 9, Histogram comparison of mismatched wavelet (MMW) based embedding to JSteg, Top: Saturn, middle: Cameraman, bottom: Goldhill. All images are of size 512x512; MMW distances used correspond to Figure 4-Figure 6. In the JSteg case, the peaks are lowered and the valleys are raised even with relatively low data amounts of (top and middle) 1024 and (bottom) 4096 bits, vs. the MMW technique which embeds >100Kbits many cases shown.

JSteg is freely available and widely used [31][32]. This comparison is sufficient to demonstrate the viability of this approach. The images and wavelets from Figure 4-Figure 6 were used to hide data, the number of bits modified, by the mismatched transform are shown in Figure 8. Note for distances greater than 0.5, all three images store 10^5 bits, the same images using JSteg can only embed up to 4092 bits of information. Figure 9 shows a zoom in on the histogram changes as compared to JSteg. Notice how JSteg has clear smoothing effect on peaks and leveling of valleys that is not present with the mismatched wavelet despite the embedding rate difference between the two techniques.

IV. Edge Detection

In this section we show how mismatched wavelets can be used for edge detection. Comparative results are shown in both qualitative examples and a quantitative measure using methods discussed in [33].

A. *Edge Detectors*

The detection of edges in images is a fundamental problem in image processing. Many applications such as target detection, facial recognition, or simple denoising, use edge detection as a first stage process. Typical methods of edge detection use a process of filtering, followed by the estimation of the gradient, followed by a final noise removal stage using thresholding. Three examples used here include the Sobel algorithm, which approximates horizontal and vertical gradient operators, the Prewitt algorithm which uses a set of eight

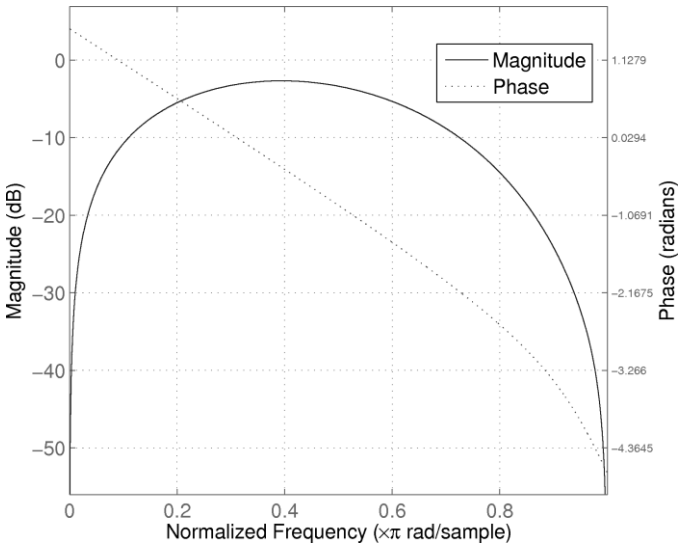

Figure 10, Filter response of *pollen(1)-pollen(2)*, the filter used for reconstruction in Figure 14 and Figure 15.

kernels to approximate a continuous gradient operator, and Canny algorithm which uses a Gaussian filter followed by four gradient estimating kernels. [33]-[35]

Here we introduce a method based on using mismatched wavelets. Similar to the preceding section this method is based on distorting the image through the systematic mechanism of mismatched wavelets. If the proper wavelets are chosen, the effect of this distortion is a simple highlighting of edges.

B. Mismatched Wavelet

The mismatched wavelet approach to edge detection again involves a distortion channel:

$$G = W_1 W_2^T . \tag{4.1}$$

In this case the wavelets used introduce distortion only on the edges of the images. The process used is similar to that discussed earlier,

1) Perform full forward DWT using W_1
2) Perform inverse DWT using W_2
3) Take the difference between the original image and the results
4) Optionally, use thresholding to remove remaining highpass noise

The example wavelets used in many of the figures here were ϕ_n and $\overset{)}{\phi}_n$ equal to Pollen(2) and Pollen(3), respectively. To make this process more efficient, given the linear nature of the operators, it is trivial to optimize this process by replacing W_2, with $W_1 - W_2$, which is equivalent to performing the inverse DWT with the non-orthonormal filter $\phi(t) - \overset{)}{\phi}(t)$. Or,

1) Perform full forward DWT using W_1 or $W_{\phi(t)}$
2) Perform inverse DWT using $W_{\phi(t)-\overset{)}{\phi}(t)}$

A proof of this optimization is found in the appendix. An example of an optimized filter is shown in Figure 10. Notice it has a clear band pass characteristic.

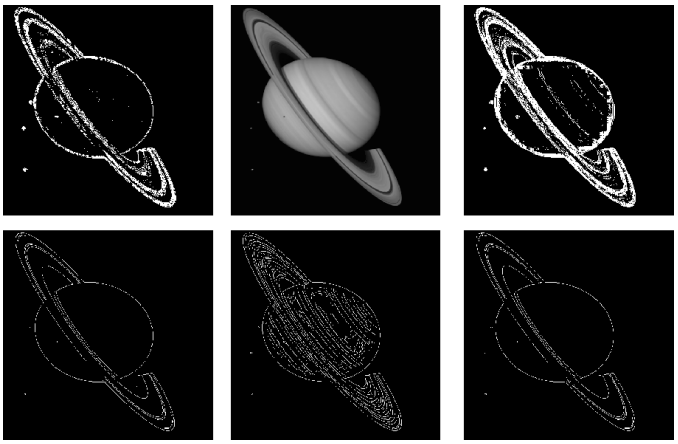

Figure 11 Edge detection comparison, Top, left to right: wavelet-based technique, original, MMW technique, Bottom, left to right: Sobel, Canny, Prewitt edge detectors.

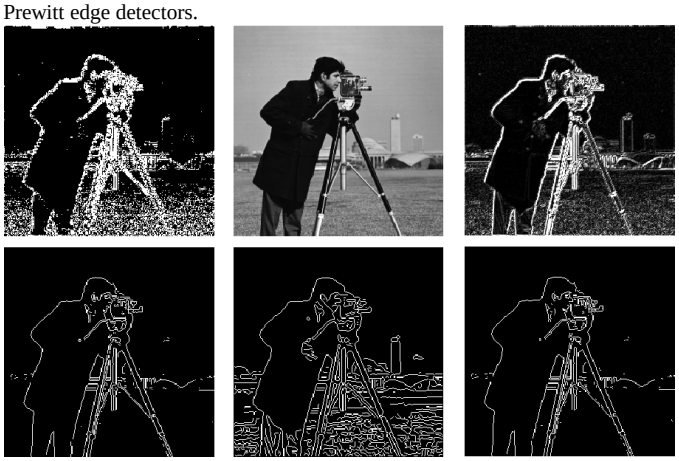

Figure 12 Edge detection comparison, Top, left to right: wavelet-based technique, original, MMW technique, Bottom, left to right: Sobel, Canny, Prewitt edge detectors.

C. Comparison

A series of experiments were performed to demonstrate the effectiveness of the mismatched wavelet approach to edge detection. These include qualitative and quantitative comparisons. In the first set of experiments, we *qualitatively* explore this approach compared to Sobel, Canny, and Prewitt methods, as well as the wavelet based method described in a the introduction of this paper. The images Saturn, Cameraman, and Goldhill were chosen as three challenging images for edge detectors. Figure 11-Figure 13, show the results from this comparison. There are several features of these images to highlight an edge detector.

In the "Saturn" image four moons are visible. In Figure 11, one is dark with Saturn as a backdrop, and the others are light just below the body of Saturn. Notice each technique does not highlight all four moons.

In "Cameraman", the presence of the airport tower in the background is often a challenge for edge detection. There are also two imperfections in this image, one above the cameraman's right elbow, the other above the tower. In Figure 12 some detectors highlight this imperfection and others do not.

The final image, Goldhill, is a challenging image for edge detection. In Figure 13 most techniques do not appear to

Figure 13 Edge detection comparison, Top, left to right: wavelet-based technique, original, MMW technique, Bottom, left to right: Sobel, Canny, Prewitt edge detectors.

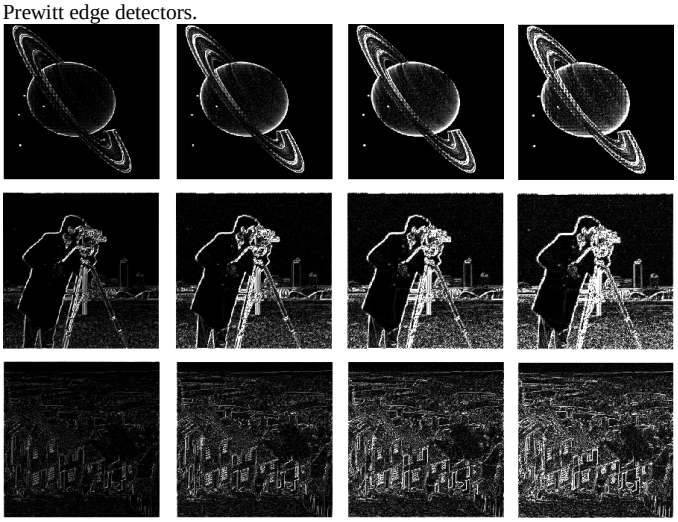

Figure 14, Edge detection performance as the wavelet used changes, left to right distances of $\frac{\pi}{11}$, $\frac{2\pi}{11}$, $\frac{3\pi}{11}$, $\frac{4\pi}{11}$. Base wavelet was $\varphi = 1$.

capture the information content in the image. The Sobel approach is very good at finding the edges, but somehow fails to convey the information content. The proposed technique communicates the shape of the houses and windows, as well as the contours in the background.

To further explore effect of wavelet distance on edge detection, Figure 14 shows distances of $\frac{\pi}{11}$, $\frac{2\pi}{11}$, $\frac{3\pi}{11}$, $\frac{4\pi}{11}$. Notice the slow change in edge detection as the distance is varied. Saturn and Cameraman seem to be best at $\frac{3\pi}{11}$, while Goldhill is best at $\frac{4\pi}{11}$. A study was also conducted with respect to threshold. Figure 15 shows how varying level of threshold affects the three images differently. A low threshold causes Saturn to simply "fill in", while Goldhill becomes almost entirely white. This implies a threshold selection mechanism based on image luminance.

Of course all measures of performance of an edge detector should be made in light of a particular application, but such an

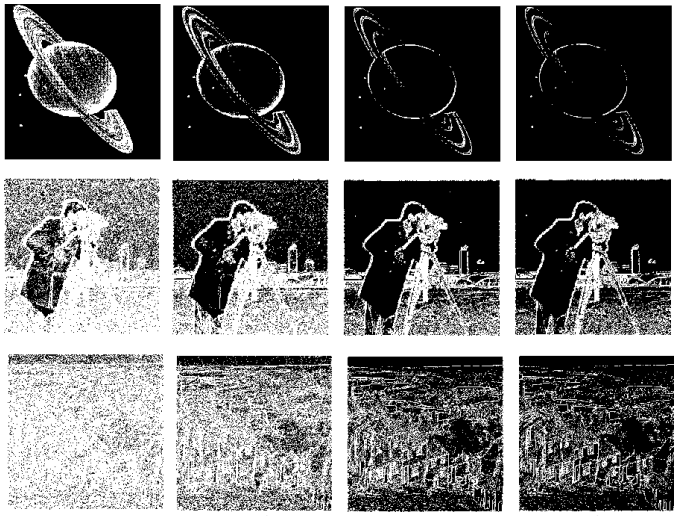

Figure 15, Edge detection performance as the threshold is varied, left to right thresholds of 1, 3, 8, 11. Base wavelet was $\varphi_A = 1, \varphi_S = 2$

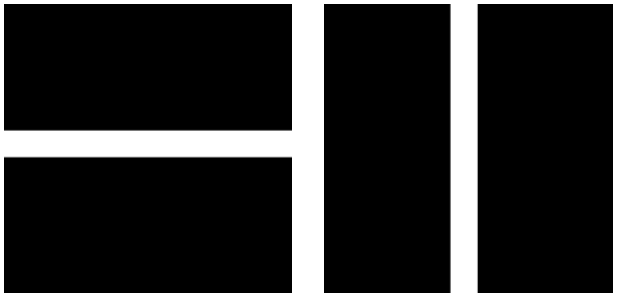

Figure 16, Clean test images for Figure 17 and Table II

evaluation is beyond the scope here. Instead to provide a *quantitative* evaluation of the proposed edge detection technique, an analysis was conducted using the two artificial images shown in Figure 16. By using two simple images, with known edges we can measure the rate of miss and false alarms. In this case the images are black with a single stripe, 3 pixels wide, in the first case the stripe is horizontal, in the second vertical. The known edges are used to quantify the performance of the edge detector. To avoid well known offset problems between the different algorithms different "ground truth" edges were used for each technique; we report the best result for each technique. For example, some algorithms, such as the Sobel and Prewitt, will tend to detect the edge on the left side of a vertical edge, while others such as the Canny algorithm, will prefer the side of the edge with less luminance. Using this known set of edges, an evaluation was made using a pixel by pixel measure of probability of miss and false alarm from [33].

$$\begin{aligned} p(miss \mid edge) &= 1 - p(\det ection \mid edge) \\ &= 1 - \frac{p(\det ection \text{ I } edge)}{p(edge)} \\ &= 1 - \frac{\#\det ection\ on\ edge}{\#edge\ \ pixels} \end{aligned} \tag{4.2}$$

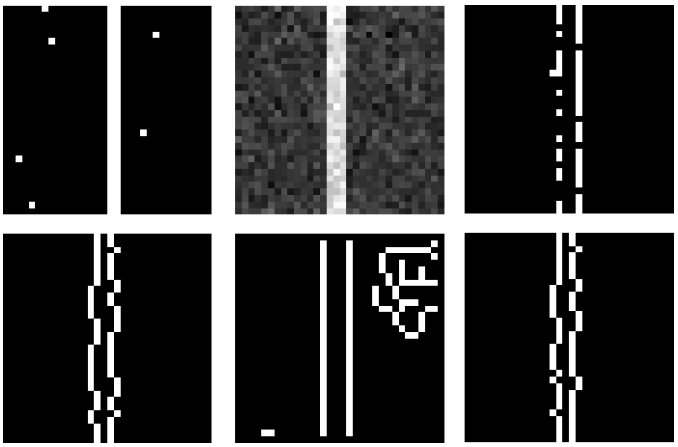

Figure 17, Example edge detection results with noise of SNR 10, Top left to right, Wavelet edge detection, Noisy image, NPR edge detection, Bottom, left to right, Sobel, Canny, Prewitt standard edge detection techniques.

$$p(\det ection \mid no\ edge) = \frac{p(\det ection \mathrm{I}\ nonedge)}{p(nonedge)} = \frac{\#\det ection\ on\ no\ edge}{\#nonedge\ pixels} \tag{4.3}$$

To evaluate the robustness of the edge detection techniques, probabilities were computed under a number of noise conditions, from integer SNR values from 1 to 10. Figure 17 shows an example result of this test at an SNR of 10. As can be seen from the Figure, the wavelet based method did not perform well on this particular image for any choice of threshold, missing one edge entirely. The NPR wavelet performed well selecting a well defined though slightly sparse edges, while the Sobel and Prewitt edges show a wavering effect due to the noise. The Canny approach did very well at selecting the true edges, but also had detections where only noise was present in the image. The resulting miss and false alarm rates are shown in Table I. For this table the probabilities were averaged across a number of simulations and across SNR. The NPR makes a compromise with a low false alarm rate and good probability of miss. For this experiments the parameters of the various edge detection techniques were not tweaked for performance, so it is likely each could potentially do better than shown here.

V. Conclusion

In this paper we introduced a new method of applying wavelets to problems in signal and image processing. This approach uses non-perfect reconstruction to create a structured distortion channel. We introduced mismatched wavelets as a basis for inducing mild distortion which maintains much of the information content of the image. In using wavelets as a foundation, we have gained the benefit of the processing speed of wavelets. This approach is applied to two important problems in signal and image processing. We demonstrate an information hiding technique based on generating a near identity distortion matrix and using this to locate embeddable pixels. This approach guarantees visual and statistical similarity. We further show how mismatched wavelets can be applied to the problem of edge detection. The results of this approach show much promise when compared to several other techniques.

Table I, Comparison of Edge Detection Techniques, mean miss and false alarm rates across two test images and 10 SNRs.

	P_m	P_{fa}
Wavelet	0.4685	0.1443
NPR	0.3724	0.0265
Sobel	0.5239	0.0310
Canny	0.2236	0.0885
Prewitt	0.5202	0.0316

Given the premise of introducing structured distortion to do something useful, the mechanism presented is far from the only solution available. Obvious extensions using biorthogonal wavelets or steerable pyramids are likely to have similar or better performance. In addition the use of wavelet packet or multiwavelet style ideas holds much unexplored potential. For applications, an open problem remains in how to optimally select or adapt the best wavelet for either analysis or synthesis.

Appendix

Theorem, The following procedure

1) Perform forward DWT using $W_{\phi(t)}$

2) Perform inverse DWT using $W_{\phi(t)}^{)}$

3) Take the difference between the original image and the results

Or, $e = W_{\phi(t)} X W_{\phi(t)}^{-1} - X$

Is equivalent to

1) Perform forward DWT using $W_{\phi(t)}$

2) Perform inverse DWT using $W_{\phi(t)-\phi(t)}^{)}$

Or, $e = W_{\phi(t)} X W_{\phi(t)-\phi(t)}^{-1)}$

Proof:

$$\begin{aligned} e &= W_{\phi(t)} X W_{\phi(t)}^{-1} - X \\ &= W_{\phi(t)} X W_{\phi(t)}^{-1} - W_{\phi(t)} X W_{\phi(t)}^{-1} \\ &= W_{\phi(t)} X (W_{\phi(t)}^{-1} - W_{\phi(t)}^{-1}) \\ &= W_{\phi(t)} X (W_{\phi(t)-\phi(t)}^{-1)}) \quad \square \end{aligned} \tag{4.4}$$

Acknowledgment

The authors would like to thank the various members of the Multimedia and Mobile Signal Processing Lab (MMSP) at UTSA for their constant source of entertainment and support.

References

[1] S. Mallat, A Wavelet Tour of Signal Processing, Academic Press, 2nd edition, 1999.

[2] B. Vidakovic, Statistical modeling by wavelets, New York: Wiley, 1999.

[3] Hardle, W., Kerkyacharian, G., Pikard, D. & Tsybakov, A. Wavelets, Approximation, and Statistical Applications. Lecture Notes in Statistics 129, New York: Springer-Verlag, 1998

[4] I. Daubechies, B. Han, A. Ron, and Z. Shen. Framelets: MRA-based constructions of wavelet frames. Appl. Comput. Harmon. Anal., 14(1):1–46, January 2003.
[5] B. Han, "On dual wavelets tight frames," *Applied Comput. Harmonic Anal.*, no. 4, pp. 380–413, 1997.
[6] C. Chui and W. He. Compactly supported tight frames associated with refinable functions. Appl. Comput. Harmon. Anal., 8(3):293–319, May 2000.
[7] W. Lawton. Tight frames of compactly supported affine wavelets. J. Math. Phys., 31:1898-1901, 1990.
[8] Neela. R. Rayavarapu, and Neelam Rup Prakash, "A Computationally Efficient Design for Prototype Filters of an M-Channel Cosine Modulated Filter Bank", Transactions On Engineering, Computing And Technology Volume 13 May 2006.
[9] Truong &. Nguyen, "Near-Perfect-Reconstruction Pseudo-QMF Banks," IEEE Trans. Sig. Process., VOL. 42, NO. 1, 1994.
[10] G. Jovanovic-Dolecek, Multirate Systems: Design and Applications, Hershey, PA: Idea Group Publishing, 200
[11] P. P. Vaidyanathan, Multirate Systems and Filter Banks. Englewood Cliffs, NJ: Prentice-Hall, 1993.
[12] Pushkar G. Patwardhan and Vikram M. Gadre, Design of Near-Perfect Reconstruction Two-Parallelogram Filter-Banks, IEEE Signal Processing Letters, Vol. 13, No. 8, August 2006
[13] J. H. Husøy and T. A. Ramstad. Application of an efficient parallel IIR filter bank to image subband coding. Signal Processing, 20(4):279–292, August 1990.
[14] Schoerkhuber, C. and Klapuri, A., " Constant-Q transform toolbox for music processing," in the 7th Sound and Music Computing Conference, Barcelona, Spain.
[15] M. P. Eckert and A. P. Bradley, "Perceptual quality metrics applied to still image compression," Signal Process., vol. 70, no. 3, pp. 177–200, Nov. 1998.
[16] T. N. Pappas and R. J. Safranek, "Perceptual criteria for image quality evaluation," in Handbook of Image Video Processing, A. Bovik, Ed. New York: Academic, 2000.
[17] S. Winkler, "Issues in vision modeling for perceptual video quality assessment,"Signal Process., vol. 78, pp. 231–252, 1999.
[18] Zhou Wang, Alan C. Bovik, Hamid R. Sheikh, and Eero P. Simoncelli, Image Quality Assessment: From Error Visibility to Structural Similarity, IEEE Transactions on Image Processing, vol. 13, no. 4, April 2004
[19] Z. Wang, E. P. Simoncelli, and A. C. Bovik, "Multi-scale structural similarity for image quality assessment," in Proc. IEEE Asilomar Conf. on Signals, Systems, and Computers, Nov. 2003.
[20] H. R. Sheikh, M. F. Sabir, and A. C. Bovik, "A Statistical Evaluation of Recent Full Reference Image Quality Assessment Algorithms", *IEEE Transactions on Image Processing*, Vol: 15 No: 11, November 2006.
[21] C.B. Smith, S. Agaian, Visually Similar Wavelets with Application to Data Hiding Systems, Proceedings of IEEE System, Man, Cybernetics Conference, 2006.
[22] Sweldens, W. Cascade applet, http://cm.bell-labs.com/who/wim/cascade/index.html.
[23] Pollen, D. (1990). *SUl*(2*; F*[*z;* 1=*z*]) for *F* a subfield of *C*, *J. Amer. Math. Soc.*,3, 611–624.
[24] D. Colella and C. Heil, Characterizations of scaling functions: Continuous Solutions, *SIAM J. Matrix Anal. Appl.*, vol. 15, pp. 496-518, 1994.
[25] Agaian, S. "Steganography& Steganalysis An Overview of Research & Challenges", Network Security and Intrusion Detection, NATO Proceedings, 29 pages, 2005.
[26] A.D. Ker, Steganalysis of LSB Matching in Grayscale Images, IEEE Signal Processing Letters, Vol. 12, No. 6, June 2005.
[27] J.J. Harmsen and W.A. Pearlman, "Steganalysis of Additive Noise Modelable Information Hiding," SPIE/IS&T Electronic Imaging 2003, Proceedings SPIE Vol. 5022, Jan. 2003
[28] Fabien A. P. Petitcolas, Ross J. Anderson and Markus G. Kuhn, Information Hiding – A Survey, Proceedings of the IEEE, special issue on protection of multimedia content, 87(7):1062-1078, July 1999.
[29] Ross J. Anderson, Fabien A.P. Petitcolas, On The Limits of Steganography, IEEE Journal of Selected Areas in Communications, 16(4):474-481, May 1998.
[30] H. R. Sheikh, and A. C. Bovik, "Image Information and Visual Quality", IEEE Transactions on Image Processing, Vol: 15 No: 2, February 2006
[31] A. Westfeld and A. Pfitzmann, "Attacks on Steganographic Systems," Proc. Information Hiding—3rd Int'l Workshop, Springer Verlag, 1999, pp. 61–76.
[32] N. Provos and P. Honeyman, "Hide and Seek: An Introduction to Steganography," IEEE Security & Privacy Magazine, May/June 2003.
[33] Pratt, W.K., Digital Image Processing: PIKS Inside, 3rd Edition, Wiley-Interscience, 2001
[34] R. Gonzalez and R. Woods Digital Image Processing, Addison Wesley, 1992
[35] Canny, J., A Computational Approach To Edge Detection, IEEE Trans. Pattern Analysis and Machine Intelligence, 8:679-714, 1986.

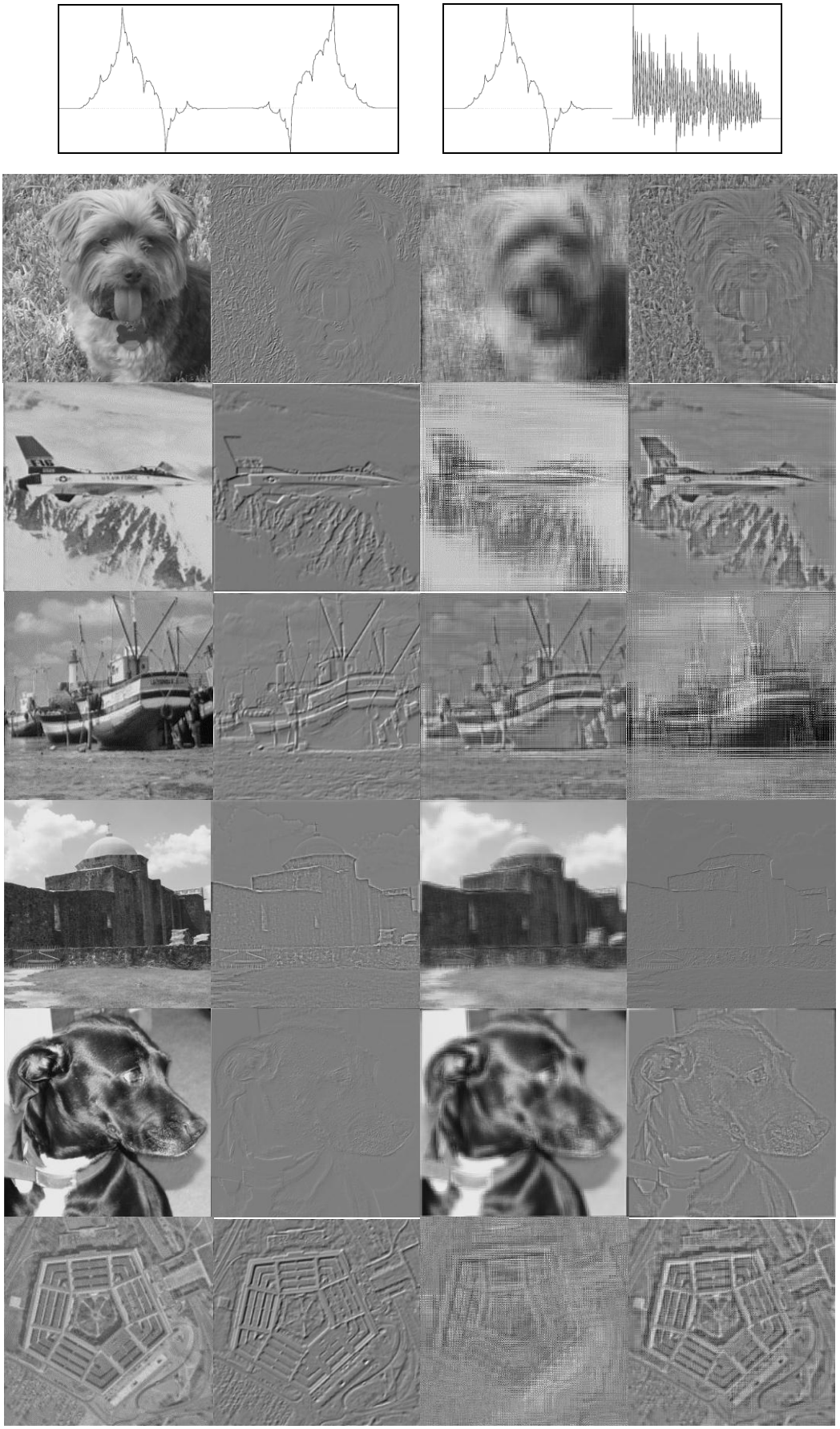

Figure 18, Example Images, Top row, wavelets used for (left) visually similar case, and (right) distorting case. Other rows, left to right on each row, visually similar reconstruction, visually similar errors, distorted reconstruction, and distorted error